Fast and Generic Energy Flow Analysis of the Integrated Electric Power and Heating Networks

Shuai Yao, Wei Gu, Jianzhong Wu, Meysam Qadrdan, Hai Lu, Shuai Lu, Yue Zhou

***Abstract*—Energy flow analysis is a fundamental tool to determine the network states of the integrated energy systems (IES). For the widely deployed IES with coupled power grids (PG) and heating networks (HN), we still lack a generic tool that can be easily employed to calculate the quasi-dynamic energy flows of it. In this paper, we have developed a generic code package (named as MATHN) for energy flow analysis of the quality-regulated HN. After that, a generic solution framework that leverages MATPOWER and MATHN to realize decomposed energy flow calculation of PG and HN is proposed. Behind the MATHN tool, a model reformulation technique is proposed to eliminate the massive indirect variables of the basic HN model discretized by finite difference, which finally derives a compact matrix formulation (similar to the network equation of power grid: $\boldsymbol{I}=\boldsymbol{YU}$) for generic description of any HN and also slashes the original model scale by around 20 times. Moreover, the solution strategy behind the MATHN tool further converts this matrix formulation into a standard system of non-homogeneous linear equations, with which some existing well-recognized algorithms can be directly applied for efficient and accurate solution. Case studies on three different scales of test systems demonstrate the generality, efficiency and accuracy of our methods. All the codes and input data are packaged into the MATHN tool and are made open-source for non-commercial use.**

***Index Terms*—Combined heat and power, Energy flow calculation, Integrated energy systems, Open-source tool, Quasi-dynamic model.**

NOMENCLATURE

Abbreviations

IES	Integrated energy system
AC	Alternating current
AE	Algebraic equation
CU	Cogeneration unit
EH-IES	Electricity and heat integrated energy system
HN	Heating network
NCES	Non-coupling electric source
NCHS	Non-coupling heating source
ODE	Ordinary differential equation
P2HU	Power-to-heat unit
PDE	Partial differential equation
PG	Power grid

Parameters

$\boldsymbol{E}_{\boldsymbol{N}_\mathrm{n}}$	The N_n-dimensional identity matrix
η^{eb}	The power-to-heat efficiency of the electric boiler
η^{bp}	The heat-to-power ratio of the back-pressure cogeneration unit
$\phi_0^{\mathrm{ec}}/P_0^{\mathrm{ec}}$	The heat / active power output of the extraction-condensing unit at the reference operating point
$\mathrm{COP}^{\mathrm{hp}}$	The coefficient of performance of the heat pump
$\varpi_{1i}/\varpi_{2i}/\varpi_{3i}$	The finite difference parameters of pipe i
B_i	A parameter of pipe i, as defined in (13)
B_i'	A parameter of pipe i, as defined in (34)
c	The specific heat capacity of hot water in the HN
L_i	The length of pipe i
N_b	The number of pipes in the HN
N_n	The number of nodes in the HN
R	The thermal resistance of each pipe
Z_t	The Z ratio of the extraction-condensing cogeneration unit at time t
$\boldsymbol{A}^+/\boldsymbol{A}^-/\boldsymbol{A}_\mathbf{n}^-$	Topology matrices of the HH, as defined in (19)
$\boldsymbol{B}_\mathbf{s}$	A parameter matrix of the HN, as defined in (34)
$\boldsymbol{C}_\mathbf{s}$	A parameter matrix of the HN, as defined in (37)
$\boldsymbol{B}_\mathbf{d}$	A parameter matrix of the HN, as defined in (23)
$\boldsymbol{C}_\mathbf{d}/\boldsymbol{D}$	Two parameter matrices of the HN, as defined in (26)

Sets

$\mathbb{E}$	The set of all the indexes of branches in a graph
$\mathbb{E}_k^{\mathrm{in}}$	The set of all the indexes of the branches connected to node k and have water flowing in
$\mathbb{E}_k^{\mathrm{out}}$	The set of all the indexes of branches that are connected to node k and have water flowing out
$\mathbb{T}$	The set of all the indexes of simulation time steps
$\mathbb{V}$	The set of all the indexes of nodes in a graph

Variables

$\boldsymbol{\phi}_\mathbf{n}^+$	The column vector consisting of $c\tilde{m}_k^+\tilde{T}_k^+$ $(k\in\mathbb{V})$
$\boldsymbol{\phi}_\mathbf{n}/\boldsymbol{T}_\mathbf{n}$	The column vector consisting of $\tilde{\phi}_k/\tilde{T}_k$ $(k\in\mathbb{V})$
$\boldsymbol{x}/\boldsymbol{g}$	Variable vectors of the HN, as defined in (31)
$(\boldsymbol{b}_\mathbf{d})^t$	A variable vector of the HN on the t^{th} temporal layer, as defined in (23)
$(\boldsymbol{c}_\mathbf{d})^t$	A variable vector of the HN on the t^{th} temporal layer, as defined in (26)
ϕ_t^{bp}	The heat power output of the back-pressure cogeneration unit at time t
ϕ_t^{eb}	The heat power output of the electric boiler at time t
ϕ_t^{ec}	The heat power output of the extraction-condensing cogeneration unit at time t
ϕ_t^{hp}	The heat power output of the heat pump at time t
τ/h	The temporal / spatial difference step size
$\tilde{\phi}$	The net injected heat power caused by the heat exchange with heat source or load at each node
$\tilde{\phi}^+$	The total injected heat power at each node caused by the injected water from outside the HN

This work was Supported by the National key Research and Development Program of China (Grant No. 2020YFE0200400) and the EPSRC through the project "Integrated heating and cooling networks with heat-sharing-enabled smart prosumers" (EP/T022795/1) (Corresponding author: Wei Gu).

$\tilde{\phi}_k$ The net injected heat power caused by the heat exchange with heat source or load at node k
$\tilde{\phi}_k^+$ The total injected heat power at node k caused by the injected water from outside the HN
$\tilde{m}$ The mass flow rate of the injected water from outside the HN at each node
$\tilde{T}$ The relative water temperature at each node
$\tilde{T}_k$ The relative water temperature at node k
$\tilde{T}_k^-$ The relative outflow water temperature at node k
b_i^t A variable of pipe i on the t^{th} temporal layer, as defined in (13)
m The mass flow rate in each pipe
M_i The number of spatial difference layers of pipe i
m_{i_k} The mass flow rate in pipe i_k
N The number of temporal difference layers of each pipe
P_t^{bp} The active electric power output of the back-pressure cogeneration unit at time t
P_t^{eb} The active electric power consumption of the electric boiler at time t
P_t^{ec} The active electric power output of the extraction-condensing cogeneration unit at time t
P_t^{hp} The active electric power consumption of the heat pump at time t
T The relative water temperature in each pipe
t The independent variable of time domain / the index of temporal difference layer
T^{a} The ambient temperature outside the heating network
$T_{i,x}^t$ The relative water temperature of pipe i on the x^{th} spatial layer and the t^{th} temporal layer
$T_{i_k}^{\text{out}}$ The relative outflow water temperature of pipe i_k
$T_{j_k}^{\text{in}}$ The relative inflow water temperature of pipe i_k
v The velocity of water flow in each pipe
x The independent variable of space domain / the index of spatial difference layer
$\boldsymbol{m}_{\mathbf{b}}$ The column vector consisting of m_i $(i \in \mathbb{E})$
$\boldsymbol{m}_{\mathbf{n}}^+/\boldsymbol{T}_{\mathbf{n}}^-$ The column vector consisting of $\tilde{m}_k^+/\tilde{T}_k^-$ $(k \in \mathbb{V})$
$\boldsymbol{T}_{\mathbf{b}}^{\mathbf{o}}/\boldsymbol{T}_{\mathbf{b}}^{\mathbf{i}}$ The column vector consisting of $T_i^{\text{out}}/T_i^{\text{in}}$ $(i \in \mathbb{E})$

I. Introduction

A. Motivations

By taking advantage of the synergies among multi-energy vectors (including electricity, heat, cooling, natural gas, hydrogen, etc), the integrated energy system (IES) can effectively improve the overall efficiency of energy utilization, reduce carbon emissions [1], and provide more flexibility resources for future power systems with an increasing proportion of renewable energy generation [2].

The electricity-heat integrated energy system (EH-IES) is one of the most common types of IES, which couples the power grid (PG) and heating network (HN) with multiple cogeneration and power-to-heat units [3]. This paper focuses on the fast simulation of coupled network states, also known as "energy flows". To achieve this, the outputs of devices in this system are usually assumed to being able to quickly follow the changes of their controllers' setpoints. By doing this, the dynamic output-adjusting processes of these devices can be ignored and the detailed dynamic models of devices can be excluded from consideration when solving the network states, which improves the overall solution efficiency but surely sacrifices some degree of accuracy.

In some occasions, such sacrifice is necessary as the solution speed far outweighs the accuracy requirement. For example, in the contingency analysis of dispatch plans or in the dynamic security operation region characterization of energy networks, energy flows need to be calculated multiple times within a short period of time, making solution efficiency critical.

Energy flow analysis on the EH-IES aims to calculate the state information of the coupled PG and HN based on the given operating boundaries, and serves as a fundamental tool to facilitate the secure operation of large-scale energy systems.

A considerable number of studies have centered on this topic in the past decade, with remarkable achievements made in problem formulation and solution strategy. The time-series AC power flow model is usually adopted to capture the state variations of PG over a time period [4–6], while the more accurate quasi-dynamic state changes of HN (including the thermal transients in each pipe) are usually modeled as a mixed system of partial differential equations (PDEs) and algebraic equations (AEs) through energy conservation analysis on the pipe control volume [6, 7]. To reduce problem scale, the PG and HN can be decoupled and solved separately with some information exchanged between each other.

Despite the fruitful theoretical achievements, we still lack a practical, generic tool that can be conveniently employed to calculate the energy flows of any given EH-IES. Most of the previous studies focus on computing the energy flows of PG and HN coupled in only one or two typical modes, and some of these case-specific methods are not easy to be implemented when shifting to a different system. In view of this, a thorough coupling analysis of PG and HN is strongly desired to breed a generic solution tool with which energy flow analysis on any given EH-IES can be carried out.

Another motivation of this paper comes from the difficulties in solving the HN model in a generic and efficient way. Typically, the quasi-dynamic energy flow model of HN contains a set of PDEs capturing the thermal transients in each pipe. When these PDEs are discretized to derive the numerical solutions of the HN model, a large quantity of temporally and spatially correlated temperature variables will be introduced, which not only increases the difficulty to obtain a matrixing model formulation that can be used to conduct generic analysis on any given HN, but also lowers the solution efficiency by introducing massive intermediate difference variables [6, 8].

Inspired by the generic model formulation of the electric power network ($\boldsymbol{I} = \boldsymbol{YU}$), we seek to reformulate the aforementioned HN model into a more generic and compact matrix equation by breaking up the spatial and temporal correlations among variables, and by eliminating some intermediate variables that will not be directly used for model solution. On this basis, we would be able to conveniently employ some mature algorithms to solve this compact HN model in a standard way.

B. Literature Review

To begin with, we would like to clarify some basic concepts. The "quasi-dynamic energy flows" for PG refer to a series of

discrete AC power flows calculated with a regular time interval (typically several minutes) in the whole simulation duration, while those for a HN refer to a set of sequential state information that contains the thermal transients but not the hydraulic transients that involve dynamic pressure propagations [9]. This definition distinguishes the "quasi-dynamic" calculation from the "dynamic" simulation that involves both thermal and hydraulic transients. This paper focuses on the quality-regulated HN, with hot water as the working medium, where the mass flow rate in each pipe is preset and remains constant while the supply temperatures at some heat sources are regulated during operation [10]. This regulation strategy has better operation stability due to its stable hydraulic conditions and is widely deployed in the primary side of HN [11].

The time-series AC power flow model is adopted in most literatures to compute the quasi-dynamic energy flows of PG, but the adopted HN model has some differences. Two types of approximation models are commonly seen in previous studies. The first one calculates the outlet temperature of a pipe by imposing the effects of water transmission delay and heat loss to environment on the inlet temperature, which is quite intuitive but has relatively lower accuracy [12–17]. The second one is called the "node method", which improves the accuracy by first discretizing the water flow into small water masses and then calculating the average temperature of all the water masses that flow in a node within a calculation time interval [18–20]. This model can calculate the dynamic temperature variations at each node, but the temperature distribution along the pipe cannot be obtained. Furthermore, it leaves out the temperature wave propagation in the pipe and therefore might cause diffusion and smearing effects on the temperatures [21].

Aside from these approximation models, a more accurate PDE model derived from energy conservation analysis on the pipe control volume is adopted in [4, 6–8, 22]. To integrate this PDE model into the energy flow calculation, the finite difference method is applied in [6], where the PDE is converted into a set of AEs by a difference scheme. However, this scheme is only of first-order accuracy and should satisfy stringent stability and convergence conditions. Another higher-order scheme is raised in [8], which also has better numerical performance owing to its unconditional stability and convergence.

Instead of descretizing the PDE in the time domain, references [7, 22] apply the Fourier and Laplace Transformations to reduce the PDE into ordinary differential equations (ODEs) in the frequency domain. With this method, analytical solutions to the thermal transients can be obtained if only the initial and boundary conditions of HN satisfy the Dirichlet Conditions and can be analytically expressed. However, such conditions may not be met in some practical systems.

For long-term simulation of a large-scale HN, the PDE model discretized by the finite difference method can introduce a huge quantity of difference variables and equations [6, 8]. Worse still, these variables are highly correlated in time and space, which means the value of a variable on a certain temporal and spatial difference layer is closely dependent on the values of other variables that lie on other temporal and spatial difference layers. These features make it hard to reformulate the HN model into a compact form of matrix equation that can be used for generic description of different networks. In other words, if the target HN changes, part of the network equations will have to be manually re-derived.

Basically, there are two general ways to realize combined energy analysis of PG and HN: 1) integrate the models of PG and HN, and solve them as a whole; 2) decouple the PG and HN at the coupling facilities and solve each model separately (sometimes iteratively until a globally convergent solution is achieved). For the studies with the approximation HN models, integrated solution can be tractable if the iterative matrix is well-conditioned [23–28], while the decoupled way of solution can also see good performance [5, 29–33]. But for the PDE model after discretization, the decoupled way of solution is more achievable due to the problem scale of the discretized equations, which is adopted in [4, 6–8, 22]. Nevertheless, depending on the types and numbers of coupling facilities that serve as the slack source, the PG and HN may couple in different ways, which will substantially affect the calculation sequence of PG and HN [8]. Therefore, a thorough analysis on the coupling mechanisms of PG and HN needs to be carried out first so that a generic quasi-dynamic energy flow calculation tool for any EH-IES can be further developed.

Our previous work in [8] has presented a basic study on the quasi-dynamic energy flow calculation of PG and HN, covering the topics of model formulation, coupling analysis, node type classification, matching different timescales and a Decomposition-Iteration solution algorithm. This paper is an extension and improvement of it. We aim to improve the formulation of the discretized PDE model and develop a generic tool (named as MATHN) that can be easily called in practice to carry out energy flow analysis on any given HN. Based on this tool and the thorough coupling analysis in [8], we can further develop a generic solution framework that leverages MATPOWER [34] and MATHN to calculate the energy flows of PG and HN coupled in any mode.

C. Contributions

The contributions of this paper are summarized as follows.

1) A model reformulation technique is proposed to reformulate the discretized HN model into a generic and compact matrix equation (similar to the network equation of power grid: $\boldsymbol{I} = \boldsymbol{YU}$), which reduces the problem scale by around 20 times through slashing the indirect difference variables / equations.

2) A solution strategy is developed to convert the improved model formulation of HN into a standard system of non-homogeneous linear equations, with which some off-the-shelf algorithms can be directly applied for efficient and accurate solutions. Compared with the traditional Decomposition-Iteration algorithm, the computation time is substantially reduced and the accuracy is also slightly improved.

3) The model reformulation technique and solution strategy are encapsulated as a generic code package — MATHN, which can be easily employed to calculate the energy flows of any given HN in practice. It is also made open-source for non-commercial use.

4) A generic calculation framework that leverages MATPOWER and MATHN to realize combined energy flow analy-

sis is developed, which is simple to implement and applicable to systems with PG and HN coupled in various modes.

II. Problem Formulation

A. Basic Model of Heating Network

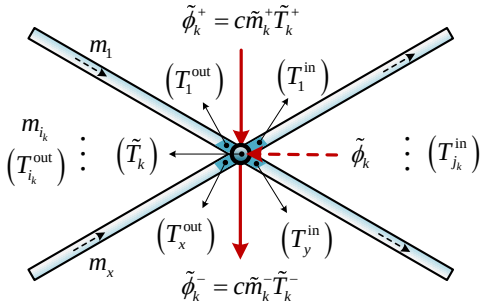

Figure 1. Schematic diagram of energy conservation at a node.

The supply and return water networks can be jointly modeled as a connected graph $G(\mathbb{V}, \mathbb{E})$, with each pipe as an edge and each node as a vertex. The quasi-dynamic model of the quality-regulated HN contains the following two parts.

1) Energy conservation at each node: the total thermal power flowing into each node equals to that flows out, as illustrated in Figure 1 and formulated in (1).

$$\begin{aligned}\sum\nolimits_{i_k\in\mathbb{E}_k^{\text{out}}}\left(m_{i_k}\cdot T_{i_k}^{\text{out}}\right)+\frac{\tilde{\phi}_k+\tilde{\phi}_k^+}{c}\\ =\tilde{T}_k\cdot\sum\nolimits_{i_k\in\mathbb{E}_k^{\text{out}}}\left(m_{i_k}+\tilde{m}_k^+\right),\ (\forall k\in\mathbb{V})\end{aligned}\tag{1}$$

where the variable m is the mass flow rate in each branch; T is the relative water temperature in each branch (calculated by the original water temperature minus the ambient temperature T^{a}); $\tilde{\phi}$ is the net injected heat power caused by the heat exchange with heat source or load at each node (the sign of $\tilde{\phi}$ being "+" / "−" means there is heat power flowing into / out of the node); $\tilde{\phi}^+$ is the total injected heat power caused by the injected water from outside the HN; $\tilde{T}$ is the relative water temperature at each node (calculated by the original water temperature minus T^{a}); $\tilde{m}$ is the mass flow rate of the injected water from outside the HN at each node. The subscript i / k denotes the index of the branch / node in the HN, while a physical variable with the superscript "out" / "+" means that it is a variable that flows out of a **branch** / flows into a **node**. The set $\mathbb{V}$ / $\mathbb{E}$ contains all the indexes of node / branch; $\mathbb{E}_k^{\text{out}}$ contains all the indexes of branches that are connected to node k and have water flowing out. The parameter c is the specific heat capacity of hot water in the HN.

After flow mixing at each node, the temperatures of those water masses that flow into the subordinate pipes or that are extracted out of the HN should be equal to $\tilde{T}$, which yields:

$$\begin{cases}T_{j_k}^{\text{in}}=\tilde{T}_k,\ \left(\forall k\in\mathbb{V},\ j_k\in\mathbb{E}_k^{\text{in}}\right)\\ \tilde{T}_k^-=\tilde{T}_k,\ (\forall k\in\mathbb{V})\end{cases}\tag{2}$$

where the subscript j denotes the index of branch, while a physical variable with the superscript "in" / "−" means that it is a variable that flows into a **branch** / flows out of a **node**. The set $\mathbb{E}_k^{\text{in}}$ contains all the indexes of the branches connected to node k and have water flowing in.

To help better understand the meaning of different variables in (1) and (2), Figure 1 is used as an illustrative case, where the target node is numbered as k. In this figure, hot water in a total number of x pipes flows into node k, and that in a total number of y pipes flows out. The symbol i_k and j_k denote the index of these pipes. In this case, (1) can be specified as:

$$\begin{aligned}m_1\cdot T_1+m_2\cdot T_2+\cdots+m_x\cdot T_x+\frac{\tilde{\phi}_k}{c}+\tilde{m}_k^+\cdot\tilde{T}_k^+\\ =\tilde{T}_k\cdot(m_1+m_2+\cdots+m_x)\end{aligned}\tag{3}$$

Equation (2) can be specified as:

$$\begin{cases}T_1^{\text{in}}=\tilde{T}_k\\ T_2^{\text{in}}=\tilde{T}_k\\ \quad\cdots\\ T_y^{\text{in}}=\tilde{T}_k\\ \tilde{T}_k^-=\tilde{T}_k\end{cases}\tag{4}$$

2) Energy conservation in each pipe: the time-variant temperature distribution of each pipe satisfies the following partial differential equation, which is derived based on the energy conservation analysis on the pipe control volume:

$$\frac{\partial T_i}{\partial t}+v_i\frac{\partial T_i}{\partial x}+\frac{v_i}{m_icR_i}T_i=0,\ (\forall i\in\mathbb{E})\tag{5}$$

where v is the velocity of water flow in each branch; R is the thermal resistance of each branch; t / x is the independent variable of time / space domain.

The finite difference method is adopted and a difference scheme developed in our previous work [35] is employed here to discretize the PDEs in (5) into a set of AEs:

$$\begin{aligned}T_{i,x+1}^{t+1}=\varpi_{1i}\cdot T_{i,x}^t+\varpi_{2i}\cdot T_{i,x}^{t+1}+\varpi_{3i}\cdot T_{i,x+1}^t,\\ (i=1,2,\cdots,N_{\text{b}};\ x=0,1,\cdots,M_i-1;\ t=0,1\cdots,N-1)\end{aligned}\tag{6}$$

where T denotes T_{b} for simplicity; N_{b} is the total number of pipes in the HN (and the total number of nodes is denoted as N_{n}); M_i is the number of spatial difference segments of pipe i; N is the number of temporal difference layers of each pipe, which is also the total simulation time steps; t / x is the index of the temporal difference layer / spatial difference segment; ϖ_{1i} – ϖ_{3i} are three constant parameters of pipe i defined for simplified representation:

$$\begin{aligned}\varpi_{1i}&=\left(1+\tfrac{v_i\tau}{h_i}-\tfrac{v_i\tau}{2m_icR_i}\right)\Big/\left(1+\tfrac{v_i\tau}{h_i}+\tfrac{v_i\tau}{2m_icR_i}\right)\\ \varpi_{2i}&=\left(\tfrac{v_i\tau}{h_i}-1-\tfrac{v_i\tau}{2m_icR_i}\right)\Big/\left(1+\tfrac{v_i\tau}{h_i}+\tfrac{v_i\tau}{2m_icR_i}\right)\\ \varpi_{3i}&=\left(1-\tfrac{v_i\tau}{h_i}-\tfrac{v_i\tau}{2m_icR_i}\right)\Big/\left(1+\tfrac{v_i\tau}{h_i}+\tfrac{v_i\tau}{2m_icR_i}\right)\end{aligned}\tag{7}$$

where τ / h is the temporal / spatial difference step size.

Through the discretization in both space and time, the difference scheme in (6) can calculate the dynamic temperature propagations in each pipe layer by layer. More specifically, the water temperature at the $(x+1)^{\text{th}}$ space segment, $(t+1)^{\text{th}}$ time layer can be calculated by a linear combination of the water temperatures at some other space and time layers, i.e. T_x^t, T_x^{t+1} and T_{x+1}^t. The detailed derivation process of (6)

can be referred to in [35], where the theoretical proof on the stability and convergence of this scheme is also given.

B. Models of Power Grid and Coupling Facilities

The time-series AC power flow model is adopted to describe the quasi-dynamics of power grid states by a series of steady-state variations, which is a well-known model that can be referred to in [8].

The PG and HN are interconnected through a group of coupling facilities including the back-pressure / extraction-condensing cogeneration units, electric boilers and heat pumps, the models of which are presented in (8) – (11).

$$\phi_t^{\mathrm{bp}} = P_t^{\mathrm{bp}} \cdot \eta^{\mathrm{bp}},\ (\forall t \in \mathbb{T}) \tag{8}$$

$$Z_t = \frac{\phi_t^{\mathrm{ec}} - \phi_0^{\mathrm{ec}}}{P_0^{\mathrm{ec}} - P_t^{\mathrm{ec}}},\ (\forall t \in \mathbb{T}) \tag{9}$$

$$\phi_t^{\mathrm{eb}} = P_t^{\mathrm{eb}} \cdot \eta^{\mathrm{eb}},\ (\forall t \in \mathbb{T}) \tag{10}$$

$$\phi_t^{\mathrm{hp}} = P_t^{\mathrm{hp}} \cdot \mathrm{COP}^{\mathrm{hp}},\ (\forall t \in \mathbb{T}) \tag{11}$$

where the set $\mathbb{T}$ contains all the indexes of simulation time steps. The superscript "bp" / "ec" / "eb" / "hp" denotes the back-pressure unit / extraction-condensing unit / electric boiler / heat pump. The parameter η^{bp} / η^{eb} / $\mathrm{COP}^{\mathrm{hp}}$ denotes the heat-to-power ratio / power-to-heat conversion efficiency / coefficient of performance; Z_t is the Z ratio used to quantify the increased heat recovery and reduced electric power output of a cogeneration unit operated under the partially condensing mode [36]. ϕ_0^{ec} / P_0^{ec} denotes the heat / electric power output of the reference operating point.

C. Coupling Mechanism and Solution Framework

To ensure the total electric/heat power generations and demands are well balanced, a slack bus/node is needed in each subsystem to eliminate the net power mismatch through increasing or decreasing its injected power generations. The slack bus/node can be played by both coupling and non-coupling facilities. Under the decoupling solution framework of energy flow analysis, the role that coupling facilities play will essentially influence the solution sequence of PG and HN models. To better explain the coupling mechanism between PG and HN, it is necessary to first understand the following assumptions and premises.

- There is only one slack bus/node for each subsystem. The setting of multi slack buses/nodes in each subsystem is not commonly seen in practical scenarios, which will significantly complicate the coupling between PG and HN. Therefore, a thorough coupling analysis under the former setting is specifically focused on in this paper.
- The slack bus of PG can be played by a non-coupling electric source (NCES, e.g., a coal-fired generator) or a cogeneration unit (CU).
- The slack node of HN can be played by a non-coupling heating source (NCHS, e.g., a coal-fired boiler), a cogeneration unit, or a power-to-heat unit (P2HU, e.g., a heat pump or an electric boiler, etc.).
- One cogeneration unit cannot simultaneously serve as the slack bus of PG and the slack node of HN. This is because the heat and electric outputs of the cogeneration unit are strongly correlated and such configuration will restrict the adjusting flexibility in both subsystems.

It can be concluded from above that the slack bus of PG can be selected from a NCES or CU, while the slack node of HN has three choices: a NCHS, CU, or P2HU. Therefore, a total of six modes can be enumerated to describe the coupling relationship between PG and HN, as detailed in Table I.

Table I
COUPLING MODES OF PG AND HN

Index	Slack bus of PG	Slack node of HN	Solution sequence
#1	NCES	NCHS	HN→PG / PG→HN
#2	NCES	CU	HN→PG
#3	NCES	P2HU	HN→PG
#4	CU	NCHS	PG→HN
#5	CU1	CU2	PG→HN→PG$\cdots$
#6	CU	P2HU	PG→HN→PG$\cdots$

In mode #1, since no coupling facilities serve as the slack bus of PG and the slack node of HN, the heat power outputs and the active electric power inputs (or outputs) of these coupling facilities are all given inputs to the energy flow models. This means the solution of both energy flow models does not rely on any information exchanged from the other subsystem, i.e., the PG and HN are already decoupled. In this scenario, the network states of PG and HN can be obtained via solving each energy flow model separately. The solution sequence can be PG first and HN second or vice versa, as presented in the last column of Table I.

In modes #2 and #3, since one coupling facility (either a CU or P2HU) serves as the slack node of HN, the active electric power input (or output) of it cannot be determined until its heat power output is obtained through solving the energy flow model of HN. Therefore, the solution sequence in this scenario should be HN first and PG second.

The situation in modes #4 is right the opposite of that in mode #2 and #3. since one cogeneration unit serves as the slack bus of PG, the heat power output of it remains unknown until its electric power output is obtained through solving the energy flow model of PG. In this scenario, the solution sequence should be PG first and HN second.

As for mode #5 and #6, the couplings get more complicated as both the slack bus and node are played by an independent coupling facility. In such cases, a feasible solution sequence could be: 1) make an initial guess on the electric power output of the cogeneration unit served as the slack bus of PG; 2) solve the energy flow model of HN to get the heat power output of the slack node of HN; 3) solve the energy flow model of PG to get an updated value of the electric power output of the slack bus of PG; 4) check if the difference between the updated value and the initial guess in 1) is within the error tolerance. If so, terminate the whole solution process and output the calculated energy flows. Otherwise, repeat 2) and 3) with the updated value in 3) until 4) is satisfied.

A generic solution framework to realize a decomposed way of solving the energy flows of PG and HN is depicted in Figure 2, where the MATPOWER and our self-developed

$$\begin{aligned} T_{i,x+1}^{t+1} &= \varpi_{1i} T_{i,x}^{t} + \varpi_{2i} T_{i,x}^{t+1} + \varpi_{3i} T_{i,x+1}^{t} \\ &= \varpi_{1i} T_{i,x}^{t} + \varpi_{2i} \left(\varpi_{1i} T_{i,x-1}^{t} + \varpi_{2i} T_{i,x-1}^{t+1} + \varpi_{3i} T_{i,x}^{t} \right) + \varpi_{3i} T_{i,x+1}^{t} \\ &= \cdots \\ &= \varpi_{2i}^{x+1} T_{i,0}^{t+1} + \varpi_{3i} T_{i,x+1}^{t} + \left(\varpi_{1i} + \varpi_{2i} \varpi_{3i} \right) \sum_{s=0}^{x-1} \varpi_{2i}^{s} T_{i,x-s}^{t} + \varpi_{2i}^{x} \varpi_{1i} T_{i,0}^{t} \end{aligned} \tag{12}$$

$$T_{i,M_i}^{t+1} = \underbrace{\varpi_{2i}^{M_i}}_{B_i} T_{i,0}^{t+1} + \underbrace{\varpi_{3i} T_{i,M_i}^{t} + \left(\varpi_{1i} + \varpi_{2i} \varpi_{3i} \right) \sum_{s=0}^{M_i-2} \varpi_{2i}^{s} T_{i,M_i-1-s}^{t} + \varpi_{2i}^{M_i-1} \varpi_{1i} T_{i,0}^{t}}_{b_i^t} \tag{13}$$

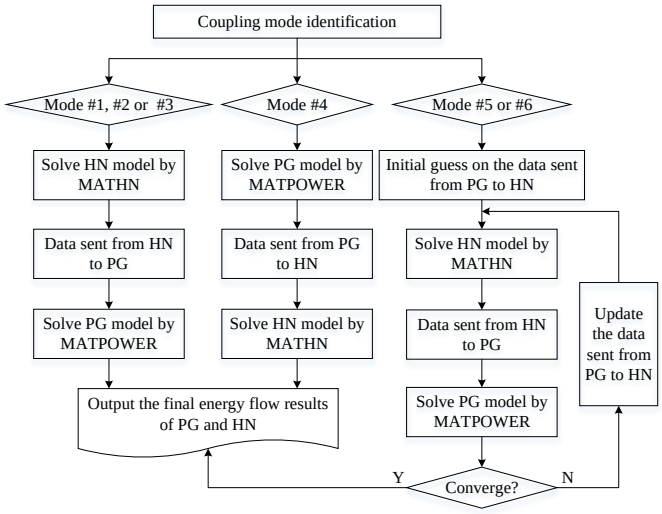

Figure 2. Generic solution framework for different coupling modes.

MATHN are employed to solve the energy flow models of PG and HN respectively.

In the first four coupling modes, owing to the relatively weak coupling between PG and HN — only one or no coupling facility serves as the slack source of PG or HN, both MATPOWER and MATHN are only called once and the final energy flow results can be obtained. In terms of the last two coupling modes, much tighter coupling appears due to the slack sources of PG and HN are both played by the coupling facilities. In this way, solving either one of the models of PG and HN would require some information from the solutions of the other model. Therefore, the energy flows of PG and HN have to be iteratively updated until a global convergence is obtained. It should be noted that timescale mismatches can occur in the process of data exchange between PG and HN, so the timescale matching strategy proposed in [8] is also adopted here to help settle this problem.

III. Improved Representation of the Basic Heating Network Model

The basic HN model presented in Section II-A involves a large quantity of spatially and temporally correlated difference variables. We seek to break the correlations and reduce some indirect difference variables and equations. On this basis, we further reformulate the basic HN model into a compact matrix equation for generic description and standardized solution. This process includes three major steps as separately discussed in the following subsections.

A. Eliminating the Variables at Spatial Difference Segments

The detailed temperature distribution along each pipe can be obtained by solving (6), but when multiple pipes are connected to form a network, we only need the inlet and outlet temperatures of each pipe to calculate the node temperatures $\tilde{T}$ in (1). This means the water temperature at each spatially discretized segment of a pipe is an indirect variable for solving the energy flow model of HN, as is marked in Figure 3, so we start the model reformulation work from eliminating these indirect variables and establish the direct relationship between the inlet and outlet temperatures of each pipe.

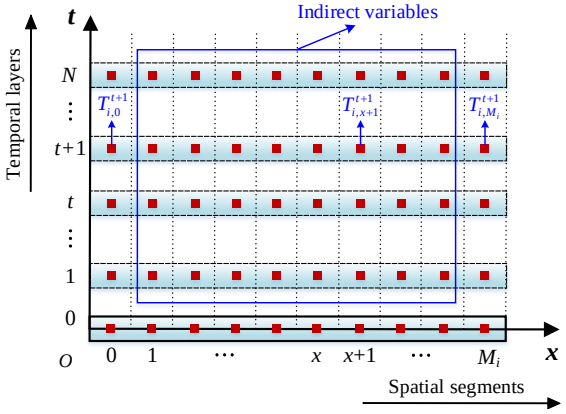

Figure 3. Schematic diagram of the finite difference grid for pipe i.

First recurse (6) by the subscript x to eliminate the temperature variables at the spatial difference segments, as presented in (12). The correctness of (12) can be examined with the Method of Mathematical Induction, as presented below.

(i) When $x = 0$, from (6) we have

$$T_{i,1}^{t+1} = \varpi_{1i} T_{i,0}^{t} + \varpi_{2i} T_{i,0}^{t+1} + \varpi_{3i} T_{i,1}^{t} \tag{14}$$

Let x in (12) be 0 and we get the same equation as (14), which means that (12) is correct when $x = 0$.

(ii) Assume (12) holds when $x = k-1$ $(k < M_i)$, so we have

$$T_{i,k}^{t+1} = \varpi_{2i}^{k} T_{i,0}^{t+1} + \varpi_{3i} T_{i,k}^{t} + \varpi_{2i}^{k-1}\varpi_{1i} T_{i,0}^{t} + \left(\varpi_{1i} + \varpi_{2i}\varpi_{3i}\right) \sum_{s=0}^{k-2} \varpi_{2i}^{s} T_{i,k-1-s}^{t} \tag{15}$$

With (15) and (6), when $x = k$ $(k < M_i)$, $T_{i,k+1}^{t+1}$ can be expressed in (16).

$$\begin{aligned} T_{i,k+1}^{t+1} &= \varpi_{1i} T_{i,k}^{t} + \varpi_{2i} T_{i,k}^{t+1} + \varpi_{3i} T_{i,k+1}^{t} \\ &= \varpi_{1i} T_{i,k}^{t} + \varpi_{2i}\left(\varpi_{2i}^{k} T_{i,0}^{t+1} + \varpi_{3i} T_{i,k}^{t} + \varpi_{2i}^{k-1}\varpi_{1i} T_{i,0}^{t}\right) \\ &\quad + \varpi_{2i}\left(\left(\varpi_{1i} + \varpi_{2i}\varpi_{3i}\right) \sum_{s=0}^{k-2} \varpi_{2i}^{s} T_{i,k-1-s}^{t}\right) + \varpi_{3i} T_{i,k+1}^{t} \end{aligned} \tag{16}$$

Further rearrange the terms in (16) and we can get

$$\begin{aligned} T_{i,k+1}^{t+1} &= \left(\varpi_{1i} + \varpi_{2i}\varpi_{3i}\right) T_{i,k}^{t} + \varpi_{3i} T_{i,k+1}^{t} + \varpi_{2i}^{k+1} T_{i,0}^{t+1} \\ &\quad + \varpi_{2i}^{k}\varpi_{1i} T_{i,0}^{t} + \left(\varpi_{1i} + \varpi_{2i}\varpi_{3i}\right) \sum_{s=0}^{k-2} \varpi_{2i}^{s+1} T_{i,k-1-s}^{t} \\ &= \varpi_{2i}^{k+1} T_{i,0}^{t+1} + \varpi_{3i} T_{i,k+1}^{t} + \varpi_{2i}^{k}\varpi_{1i} T_{i,0}^{t} \\ &\quad + \left(\varpi_{1i} + \varpi_{2i}\varpi_{3i}\right) \sum_{s=0}^{k-1} \varpi_{2i}^{s} T_{i,k-s}^{t} \end{aligned} \tag{17}$$

Equation (17) is exactly the same as (12) when $x = k$ $(k < M_i)$, which means (12) is also correct when $x = k$. From steps (i) and (ii) we can conclude that (12) is correct for all $x < M_i$.

Further replace the index of x with $(M_i - 1)$ in (12) and we can obtain the direct relationship between the outlet temperature T_{i,M_i}^{t+1} and the inlet temperature $T_{i,0}^{t+1}$ at the $(t{+}1)^{\text{th}}$ time layer, as presented in (13).

By defining the coefficient B_i and the variable b_i^t, (13) can be simply written as (18). The coefficient B_i is only dependent on $\varpi_{2,i}$ and M_i, and will remain constant on different time layers; while the variable b_i^t is calculated based on the pipe temperature distribution on the former time layer (i.e. $T_{i,x}^{t}, x = 0, 1, \cdots, M_i$) and should be updated on each time layer.

$$\begin{aligned} &T_{i,M_i}^{t+1} = B_i T_{i,0}^{t+1} + b_i^t, \\ &\quad (i = 1, 2, \cdots, N_{\text{b}};\ t = 0, 1 \cdots, N-1) \end{aligned} \tag{18}$$

B. Matrix Representation and Model Reduction

The basic HN model described by (1), (2) and (18) characterizes the energy conservation laws at each node and in each pipe, which means for each HN, a total number of $(2N_{\text{b}} + N_{\text{n}})$ equations have to be derived manually based on its topology. This is not friendly for establishing a generic energy flow calculation framework and standardized coding.

In this subsection, we will first derive the matrix representation of the basic HN model described by (1), (2) and (18), and then eliminate another set of indirect variables (the pipe inlet and outlet water temperatures: T^{in} and T^{out}) to achieve a compact HN model. Based on this, we would be able to further develop a generic energy flow calculation program which only needs to change some input parameter matrices when shifting to a different network.

First define the following topological matrices:

$$\begin{aligned} &\boldsymbol{A}^{+} = \left[a_{ki}^{+}\right]_{|\mathbb{V}|\times|\mathbb{E}|},\ a_{ki}^{+} = \begin{cases} 1, & i \in \mathbb{E}_k^{+} \\ 0, & \text{others} \end{cases} \\ &\boldsymbol{A}^{-} = \left[a_{ki}^{-}\right]_{|\mathbb{V}|\times|\mathbb{E}|},\ a_{ki}^{-} = \begin{cases} 1, & i \in \mathbb{E}_k^{-} \\ 0, & \text{others} \end{cases} \\ &\boldsymbol{A}_{\mathbf{n}}^{-} = \left[a_{\text{n},kk}^{-}\right]_{|\mathbb{V}|\times|\mathbb{V}|},\ a_{\text{n},kk}^{-} = \begin{cases} 1, & T_{\text{n},k}^{-} \neq 0 \\ 0, & \text{others} \end{cases} \end{aligned} \tag{19}$$

where $\boldsymbol{A}^{+}$ and $\boldsymbol{A}^{-}$ are two node-branch incidence matrices, while $\boldsymbol{A}_{\mathbf{n}}^{-}$ is a label matrix that marks out the nodes from which the water is extracted out of the HN.

Based on the above-defined matrices, (1) and (2) can be written in the following matrix equations:

$$\begin{aligned} &\boldsymbol{A}^{+}\text{diag}\left(\boldsymbol{m}_{\mathbf{b}}\right)\boldsymbol{T}_{\mathbf{b}}^{\mathbf{o}} + \frac{1}{c}\left(\boldsymbol{\phi}_{\mathbf{n}} + \boldsymbol{\phi}_{\mathbf{n}}^{+}\right) \\ &\qquad = \text{diag}\left(\boldsymbol{A}^{+}\boldsymbol{m}_{\mathbf{b}} + \boldsymbol{m}_{\mathbf{n}}^{+}\right)\boldsymbol{T}_{\mathbf{n}} \end{aligned} \tag{20}$$

$$\boldsymbol{T}_{\mathbf{b}}^{\mathbf{i}} = \boldsymbol{A}^{-\text{T}}\boldsymbol{T}_{\mathbf{n}} \tag{21}$$

$$\boldsymbol{T}_{\mathbf{n}}^{-} = \boldsymbol{A}_{\mathbf{n}}^{-}\boldsymbol{T}_{\mathbf{n}} \tag{22}$$

where $\boldsymbol{m}_{\mathbf{b}}$ / $\boldsymbol{T}_{\mathbf{b}}^{\mathbf{o}}$ / $\boldsymbol{T}_{\mathbf{b}}^{\mathbf{i}}$ is the column vector consisting of m_i / T_i^{out} / T_i^{in} $(i \in \mathbb{E})$, while $\boldsymbol{\phi}_{\mathbf{n}}$ / $\boldsymbol{\phi}_{\mathbf{n}}^{+}$ / $\boldsymbol{m}_{\mathbf{n}}^{+}$ / $\boldsymbol{T}_{\mathbf{n}}$ / $\boldsymbol{T}_{\mathbf{n}}^{-}$ is the column vector consisting of $\tilde{\phi}_k$ / $c\tilde{m}_k^{+}\tilde{T}_k^{+}$ / $\tilde{m}_k^{+}$ / $\tilde{T}_k$ / $\tilde{T}_k^{-}$ $(k \in \mathbb{V})$. The function $\text{diag}\left(\boldsymbol{v}\right)$ returns a square diagonal matrix with the elements of vector $\boldsymbol{v}$ on the main diagonal. The superscript "T" denotes the matrix transpose operator.

To further extend the pipe energy conservation equations in (18) from **a single pipe** to the **whole network** level, the following matrix and vector are defined:

$$\boldsymbol{B}_{\mathbf{d}} = \begin{bmatrix} B_1 & 0 & \cdots & 0 \\ 0 & B_2 & \cdots & 0 \\ \vdots & \vdots & \ddots & \vdots \\ 0 & 0 & \cdots & B_{N_{\text{b}}} \end{bmatrix},\ \left(\boldsymbol{b}_{\mathbf{d}}\right)^{t} = \begin{bmatrix} b_1^t \\ b_2^t \\ \vdots \\ b_{N_{\text{b}}}^t \end{bmatrix},\ (t \in \mathbb{T}) \tag{23}$$

Therefrom (18) can be extended as:

$$\left(\boldsymbol{T}_{\mathbf{b}}^{\mathbf{o}}\right)^{t+1} = \boldsymbol{B}_{\mathbf{d}}\left(\boldsymbol{T}_{\mathbf{b}}^{\mathbf{i}}\right)^{t+1} + \left(\boldsymbol{b}_{\mathbf{d}}\right)^{t},\ (t \in \mathbb{T}) \tag{24}$$

By now, the basic HN model has been reformulated into 4 matrix equations: (20) – (22) and (24), where the variables include $\boldsymbol{T}_{\mathbf{b}}^{\mathbf{o}}$ / $\boldsymbol{\phi}_{\mathbf{n}}$ / $\boldsymbol{T}_{\mathbf{n}}$ / $\boldsymbol{T}_{\mathbf{b}}^{\mathbf{i}}$ / $\boldsymbol{T}_{\mathbf{n}}^{-}$.

Substitute (21) and (24) into (20) to eliminate $\boldsymbol{T}_{\mathbf{b}}^{\mathbf{i}}$ and $\boldsymbol{T}_{\mathbf{b}}^{\mathbf{o}}$, and we can further obtain the direct relationship between the nodal outflow temperature vector $\boldsymbol{T}_{\mathbf{n}}$ and the nodal net injected heat power vector $\boldsymbol{\phi}_{\mathbf{n}}$ as:

$$\boldsymbol{C}_{\mathbf{d}}\left(\boldsymbol{T}_{\mathbf{n}}\right)^{t+1} + \boldsymbol{D}\left(\boldsymbol{\phi}_{\mathbf{n}}\right)^{t+1} + \left(\boldsymbol{c}_{\mathbf{d}}\right)^{t} = \boldsymbol{0},\ (t \in \mathbb{T}) \tag{25}$$

where:

$$\begin{cases} \boldsymbol{C}_{\mathbf{d}} = \boldsymbol{A}^{+}\text{diag}\left(\boldsymbol{m}_{\mathbf{b}}\right)\boldsymbol{B}_{\mathbf{d}}\boldsymbol{A}^{-\text{T}} - \text{diag}\left(\boldsymbol{A}^{+}\boldsymbol{m}_{\mathbf{b}} + \boldsymbol{m}_{\mathbf{n}}^{+}\right) \\ \boldsymbol{D} = \dfrac{1}{c}\boldsymbol{E}_{\boldsymbol{N}_{\mathbf{n}}} \\ \left(\boldsymbol{c}_{\mathbf{d}}\right)^{t} = \dfrac{1}{c}\boldsymbol{\phi}_{\mathbf{n}}^{+} + \boldsymbol{A}^{+}\text{diag}\left(\boldsymbol{m}_{\mathbf{b}}\right)\left(\boldsymbol{b}_{\mathbf{d}}\right)^{t},\ (t \in \mathbb{T}) \end{cases} \tag{26}$$

where $\boldsymbol{E}_{N_\mathrm{n}}$ is the N_n-dimensional identity matrix in (26).

Matrix equation (25) is the final reduced representation of the basic HN model, which only contains the number of N_n equations on each time layer. The energy flow of HN can be obtained by first solving (25) at each simulation time step to get the values of $\boldsymbol{T}_\mathbf{n}$ and $\boldsymbol{\phi}_\mathbf{n}$, and then using $\boldsymbol{T}_\mathbf{n}$ to compute the values of $\boldsymbol{T}_\mathbf{b}^\mathrm{i}$, $\boldsymbol{T}_\mathbf{n}^-$ and $\boldsymbol{T}_\mathbf{b}^\mathrm{o}$ through (21), (22) and (24).

C. Solution Strategy

This subsection focuses on how to efficiently solve (25). At each simulation time step, (25) contains the number of N_n equations, but the dimensions of variable vectors $\boldsymbol{T}_\mathbf{n}$ and $\boldsymbol{\phi}_\mathbf{n}$ add up to $2N_\mathrm{n}$. This means the values of N_n variables in $\boldsymbol{T}_\mathbf{n}$ and $\boldsymbol{\phi}_\mathbf{n}$ have to be specified in order to uniquely determine the solution to (25).

For a quality-regulated HN, the nodes connected to the slack heat sources will maintain specified supply temperatures — they are classified as T_n or slack node, while the others will maintain specified net injected heat power (classified as ϕ_n node) [8]. Since every node has either its T_n or ϕ_n specified, the total number of unknown variables in (25) turns to be N_n and we can proceed to obtain its unique solution.

Let $\boldsymbol{T}_\mathbf{n}^\mathbf{g}$ / $\boldsymbol{\phi}_\mathbf{n}^\mathbf{g}$ be the vector that consists of all the known variables in $\boldsymbol{T}_\mathbf{n}$ / $\boldsymbol{\phi}_\mathbf{n}$ (arranged in ascending order by their node indexes). Let $\boldsymbol{T}_\mathbf{n}^\mathbf{x}$ / $\boldsymbol{\phi}_\mathbf{n}^\mathbf{x}$ be the vector that consists of all the unknown variables in $\boldsymbol{T}_\mathbf{n}$ / $\boldsymbol{\phi}_\mathbf{n}$ (arranged in ascending order by their node indexes). Through elementary row transformation of matrix, $\boldsymbol{T}_\mathbf{n}$ and $\boldsymbol{\phi}_\mathbf{n}$ can be expressed as:

$$\boldsymbol{T}_\mathbf{n} \overset{\mathrm{r}}{\sim} \begin{bmatrix} \boldsymbol{T}_\mathbf{n}^\mathbf{x} \\ \hdashline \boldsymbol{T}_\mathbf{n}^\mathbf{g} \end{bmatrix}, \ \boldsymbol{\phi}_\mathbf{n} \overset{\mathrm{r}}{\sim} \begin{bmatrix} \boldsymbol{\phi}_\mathbf{n}^\mathbf{x} \\ \hdashline \boldsymbol{\phi}_\mathbf{n}^\mathbf{g} \end{bmatrix} \tag{27}$$

where the operator $\overset{\mathrm{r}}{\sim}$ denotes the elementary row transformation of matrix.

Similarly, let $\boldsymbol{C}_\mathbf{d}^\mathbf{g}$ / $\boldsymbol{D}^\mathbf{g}$ be the matrix that consists of all the known variable columns in $\boldsymbol{C}_\mathbf{d}$ / $\boldsymbol{D}$ (arranged in ascending order by their column indexes). Let $\boldsymbol{C}_\mathbf{d}^\mathbf{x}$ / $\boldsymbol{D}^\mathbf{x}$ be the matrix that consists of all the unknown variable columns in $\boldsymbol{C}_\mathbf{d}$ / $\boldsymbol{D}$ (arranged in ascending order by their column indexes). Through elementary column transformation of matrix, $\boldsymbol{C}_\mathbf{d}$ and $\boldsymbol{D}$ can be expressed as:

$$\boldsymbol{C}_\mathbf{d} \overset{\mathrm{c}}{\sim} \left[\boldsymbol{C}_\mathbf{d}^\mathbf{x} \vdots \boldsymbol{C}_\mathbf{d}^\mathbf{g} \right], \ \boldsymbol{D} \overset{\mathrm{c}}{\sim} \left[\boldsymbol{D}^\mathbf{x} \vdots \boldsymbol{D}^\mathbf{g} \right] \tag{28}$$

where the operator $\overset{\mathrm{c}}{\sim}$ denotes the elementary column transformation of matrix.

From (27) and (28), we have:

$$\begin{cases} \boldsymbol{C}_\mathbf{d}\boldsymbol{T}_\mathbf{n} = \boldsymbol{C}_\mathbf{d}^\mathbf{x}\boldsymbol{T}_\mathbf{n}^\mathbf{x} + \boldsymbol{C}_\mathbf{d}^\mathbf{g}\boldsymbol{T}_\mathbf{n}^\mathbf{g} \\ \boldsymbol{D}\boldsymbol{\phi}_\mathbf{n} = \boldsymbol{D}^\mathbf{x}\boldsymbol{\phi}_\mathbf{n}^\mathbf{x} + \boldsymbol{D}^\mathbf{g}\boldsymbol{\phi}_\mathbf{n}^\mathbf{g} \end{cases} \tag{29}$$

Substitute (29) into (25), and we get:

$$\begin{aligned} &\boldsymbol{C}_\mathbf{d}^\mathbf{x}\left(\boldsymbol{T}_\mathbf{n}^\mathbf{x}\right)^{t+1} + \boldsymbol{C}_\mathbf{d}^\mathbf{g}\left(\boldsymbol{T}_\mathbf{n}^\mathbf{g}\right)^{t+1} + \boldsymbol{D}^\mathbf{x}\left(\boldsymbol{\phi}_\mathbf{n}^\mathbf{x}\right)^{t+1} \\ &\quad + \boldsymbol{D}^\mathbf{g}\left(\boldsymbol{\phi}_\mathbf{n}^\mathbf{g}\right)^{t+1} + \left(\boldsymbol{c}_\mathbf{d}\right)^t = \mathbf{0}, \ (t \in \mathbb{T}) \end{aligned} \tag{30}$$

By defining the following vectors and matrices

$$\begin{aligned} \boldsymbol{x} &= \begin{bmatrix} \boldsymbol{T}_\mathbf{n}^\mathbf{x} \\ \hdashline \boldsymbol{\phi}_\mathbf{n}^\mathbf{x} \end{bmatrix}, \ \boldsymbol{g} = \begin{bmatrix} \boldsymbol{T}_\mathbf{n}^\mathbf{g} \\ \hdashline \boldsymbol{\phi}_\mathbf{n}^\mathbf{g} \end{bmatrix}, \\ \boldsymbol{F}_\mathbf{d}^\mathbf{x} &= \left[\boldsymbol{C}_\mathbf{d}^\mathbf{x} \vdots \boldsymbol{D}^\mathbf{x} \right], \ \boldsymbol{F}_\mathbf{d}^\mathbf{g} = \left[\boldsymbol{C}_\mathbf{d}^\mathbf{g} \vdots \boldsymbol{D}^\mathbf{g} \right] \end{aligned} \tag{31}$$

Equation (30) can be reformulated into the following form:

$$\boldsymbol{F}_\mathbf{d}^\mathbf{x}\left(\boldsymbol{x}\right)^{t+1} + \boldsymbol{F}_\mathbf{d}^\mathbf{g}\left(\boldsymbol{g}\right)^{t+1} + \left(\boldsymbol{c}_\mathbf{d}\right)^t = \mathbf{0}, \ (t \in \mathbb{T}) \tag{32}$$

It can be seen that $\boldsymbol{x}$ consists of all the unknown variables in $\boldsymbol{T}_\mathbf{n}$ and $\boldsymbol{\phi}_\mathbf{n}$, while $\boldsymbol{g}$ is a known vector consisting of all the specified variables in $\boldsymbol{T}_\mathbf{n}$ and $\boldsymbol{\phi}_\mathbf{n}$. At each simulation time step, (32) is a standard system of non-homogeneous linear equations and can be efficiently solved by calling some mature and well-recognized algorithms such as the LU factorization method.

After solving (32), we can restore the values of $\boldsymbol{T}_\mathbf{n}$ and $\boldsymbol{\phi}_\mathbf{n}$ through (27) and (31). Once $\boldsymbol{T}_\mathbf{n}$ is obtained, the values of $\boldsymbol{T}_\mathbf{b}^\mathrm{i}$, $\boldsymbol{T}_\mathbf{n}^-$ and $\boldsymbol{T}_\mathbf{b}^\mathrm{o}$ can be calculated by substituting $\boldsymbol{T}_\mathbf{n}$ into (21), (22) and (24) respectively. Further, with the inlet temperature of each pipe (i.e. the elements of $\boldsymbol{T}_\mathbf{b}^\mathrm{i}$), the temperatures at all spatial difference segments that have been eliminated before can be calculated via (12). As such, the quasi-dynamic state information of heating network can be completely obtained.

D. Summary of the Model Reformulation and Solution Steps

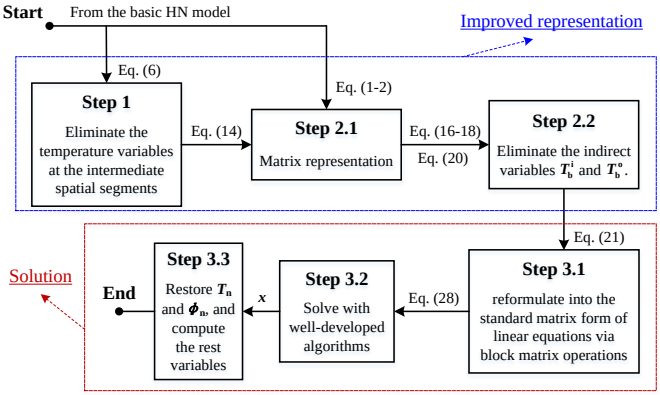

Figure 4. Flow chart for model reformulation and solution.

Major work in Section III-A - III-C is summarized into three steps in Figure 4, where the first two steps describe how to reduce and reformulate the basic HN model into a compact matrix formulation. The improved formulation, i.e., (25), is then sent to the third step for standardized solution. To ensure efficient solution of (25), the block matrix operations are employed to convert the original problem into a standard form of linear equations, which can be further solved by calling existing well-developed algorithms.

Here we have some remarks on the general reformulation and solution strategies:

Remark 1. Two sets of indirect variables are eliminated in Step 1 and 2, which significantly reduces the problem scale of calculating the energy flows of HN. For a HN with N_b pipes and N_n nodes, assume each pipe is dicretized into M spatial segments and N temporal layers, the improved formulation can reduce the total number of variables (or equations) in the HN model from $(2NMN_\mathrm{b} + N_\mathrm{n}N)$ to $N_\mathrm{n}N$. In radical networks, $N_\mathrm{b} = N_\mathrm{n} - 1$ (i.e., $N_\mathrm{b} \approx N_\mathrm{n}$), which derives that the number of equations in the basic HN model would be approximately $(2M + 1)$ times of that in the improved formulation. Assume a typical value of 10 for M and we

would see the problem scale is reduced by 20 times through our reformulation work.

Remark 2. Massive temporally and spatially correlated temperature variables are introduced due to finite difference, but the model reformulation work breaks up the couplings among different temperature variables by eliminating the indirect variables at the intermediate spatial segments, which allows to sequentially solve the HN model one time layer a time. On each time layer, the HN model is reformulated into a standard form of N_{n} dimensional linear equations (as shown in (32)) and can be efficiently solved by calling some existing mature algorithms. Both the solution efficiency and accuracy will be enhanced with the solution strategy proposed in Section III-C, which will be demonstrated through tests on different scales of systems in Section IV.

Remark 3. The improved formulation for quasi-dynamic energy flow calculation can be easily extended to calculate the steady-state energy flow. For steady-state HN, thermal transients in each pipe are neglected and we only care about the eventual system states that do not change with time. So the PDE in (5) describing the temperature dynamics in each pipe is replaced by a heat loss model that directly links the steady-state inlet and outlet water temperatures of each pipe:

$$T_i^{\mathrm{out}} = T_i^{\mathrm{in}} \cdot e^{-\frac{L_i}{m_i c R_i}}, \ (\forall i \in \mathbb{E}) \tag{33}$$

where L_i is the length of pipe i.

Let

$$B_i' = e^{-\frac{L_i}{m_i c R_i}}, \ \boldsymbol{B}_{\mathbf{s}} = \begin{bmatrix} B_1' & 0 & \cdots & 0 \\ 0 & B_2' & \cdots & 0 \\ \vdots & \vdots & \ddots & \vdots \\ 0 & 0 & \cdots & B_{N_{\mathrm{b}}}' \end{bmatrix}, \ (\forall i \in \mathbb{E}) \tag{34}$$

and (24) can be replaced by:

$$\boldsymbol{T}_{\mathbf{b}}^{\mathbf{o}} = \boldsymbol{B}_{\mathbf{s}} \boldsymbol{T}_{\mathbf{b}}^{\mathbf{i}} \tag{35}$$

Similar to the process of deriving (25), by substituting (21) and (35) into (20) to eliminate $\boldsymbol{T}_{\mathbf{b}}^{\mathbf{i}}$ and $\boldsymbol{T}_{\mathbf{b}}^{\mathbf{o}}$, we can get the improved formulation for the steady-state HN model:

$$\boldsymbol{C}_{\mathbf{s}} \boldsymbol{T}_{\mathbf{n}} + \boldsymbol{D} \boldsymbol{\phi}_{\mathbf{n}} = \mathbf{0} \tag{36}$$

where:

$$\boldsymbol{C}_{\mathbf{s}} = \boldsymbol{A}^{+} \mathrm{diag}\left(\boldsymbol{m}_{\mathbf{b}}\right) \boldsymbol{B}_{\mathbf{s}} \boldsymbol{A}^{-\mathrm{T}} - \mathrm{diag}\left(\boldsymbol{A}^{+} \boldsymbol{m}_{\mathbf{b}} + \boldsymbol{m}_{\mathbf{n}}^{+}\right) \tag{37}$$

Similar to (25), matrix equation (36) also contains the number of N_{n} linear algebraic equations and can be solved with the same strategy developed in Section III-C.

Remark 4. The improved model formulation allows for standardized coding to achieve generic energy flow calculation of any given HN. When shifting to a different network, we only need to arrange the input data (i.e., the topology and parameters of HN) by the specified data format in [37]. The standardized codes in [37] will first automatically derive $\boldsymbol{A}^{+}$, $\boldsymbol{A}^{-}$, $\boldsymbol{A}_{\mathbf{n}}^{-}$ and $\boldsymbol{m}_{\mathbf{b}}$, then do the model reformulation work and finally output the energy flows using the solution strategy discussed in Section III-C.

IV. Case Studies

In this section, the detailed procedures of energy flow calculation on a small exemplary heating network is firstly displayed to help illustrate how to implement the proposed method step by step. After that, we will demonstrate the validity and advantages of our method through tests on two different scales of EH-IES. All tests are run in MATLAB R2021a on a computer with Intel(R) Core(TM) i7-4790 CPU @3.60 GHz and 24.0 GB memory. All data and codes are shared in [37] and are open for amendments and non-commercial use.

A. Case 1: an Illustrative Case

In this case, energy flow calculation on a simple HN with 5 nodes and 6 branches is presented in detail, aiming to help readers better understand and implement the proposed method. Due to the limit of page length, we have put the detailed procedures and results in [38] for reference.

B. Case 2: EH-IES With Simple Topology

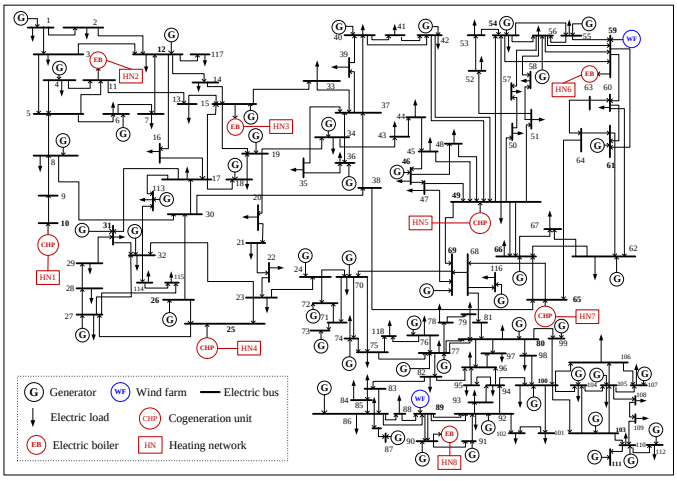

Figure 5. Diagram of the test system in Case 2.

The same test system as in [8] is used in this case, which consists of a modified IEEE 118-bus power grid and eight 35-node heating networks. The PG and HNs are coupled through 4 back-pressure cogeneration units and 4 regenerative electric boilers, as displayed in Figure 5. More specifically, the cogeneration unit at bus 11 serves as the slack node of HN1 and a PV bus of PG, so the PG and HN1 are coupled in mode #2. The cogeneration units at buses 25, 49 and 65, along with the four regenerative electric boilers at bus 11, 15, 60 and 90 serve as the PV bus of PG and do not serve as the slack node of HN, so the rest 7 HNs couple with PG in mode #1.

The overall simulation time is 300 minutes. The temporal difference step size τ is 1 minute and the spatial step sizes $h_i \, (i \in \mathbb{E})$ are dependent on the flow velocity v_i in each pipe, and satisfy $h_i = v_i \cdot \tau$. Keeping the ratio of spatial-temporal step sizes consistent with the flow velocity in each pipe can eliminate the undesired dissipation and dispersion errors introduced by finite difference. The HN model is solved with

the LU factorization method based on the improved model formulation developed in Section III, and the PG model is solved with MATPOWER 7.1.

Since 8 heating networks in this case share the same topology and parameters, we only present and discuss the quasi-dynamic energy flow results of the first HN here. The net injected heat power variations at all non-slack sources and loads are displayed in Figure 6(a), which are given conditions for energy flow calculation. Source 2 serves as the slack node of HN, with its supply water temperatures maintained at 110 °C, as shown by the orange line in Figure 6(b).

The computed heat power output of the slack source is illustrated by the black solid curve in Figure 6(a), showing how Source 2 adjusts its output to offset the system net heat power imbalance. The supply water temperatures of the other 2 sources are displayed in Figure 6(a). When the heat power output of the non-slack source rises, its supply water temperature will rise accordingly while its return water temperature will vary in an opposite manner so as to release more energy, as illustrated by the blue and magenta solid curves in Figure 6(d).

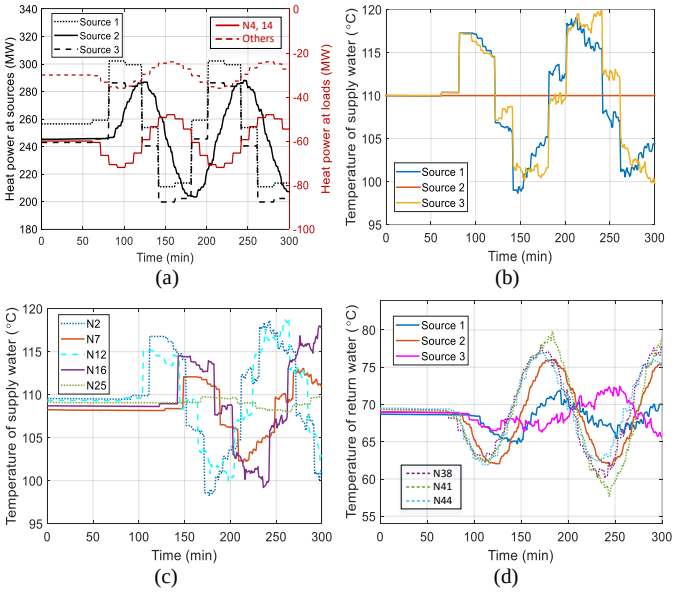

Figure 6. Energy flow results of HN: (a) Net injected heat power at source and load nodes. (b) Supply temperatures at source nodes. (c) Supply temperatures at some intermediate nodes. (d) Return temperatures at source and some intermediate nodes.

Figure 6(c) and (d) also display the supply and return water temperatures of some intermediate nodes. It should be noted that the supply and return water networks of one HN need not to be distinguished in our improved model formulation, so the nodes / pipes in both supply and return water networks are numbered together. The afore-mentioned 35-node HN actually refers to the number of nodes in the supply network, but when both the supply and return networks are numbered together, this HN should contain 46 nodes and 70 pipes. So nodes 38, 41 and 44 in Figure 6(d) actually refer to the nodes in the return network. From these two sub-figures, we can see that the supply and return water temperatures operate near the design condition (110-70 °C), demonstrating the capability of the slack source to maintain normal operation conditions.

To test the efficiency and accuracy of our improved model formulation and solution strategy, we compare the computation performances among six different solution methods that are based on both the basic and improved model formulations, as listed in Table II. The basic formulation is solved by the Decomposition-Iteration algorithm from [8], while the improved formulation is a standard system of linear equations solved with five off-the-shelf algorithms.

For the basic formulation of the first HN, it takes 1.43 seconds for the Decomposition-Iteration algorithm to obtain the final energy flow results. The convergence criteria is set to be 10^{-5}, which means the iterative solution process will terminate when the maximal deviation between two latest calculated results drops to within 10^{-5}. For the other 5 algorithms based on the improved formulation, only the LU factorization method with partially pivoting can obtain the correct solution, while the Jacobi and Gauss-Seidel iterative methods fail due to the iterative matrix being of singular working accuracy, and the Gauss Elimination method fails because zero principal diagonal elements are detected in the coefficient matrix.

The LU factorization method embedded in the “linesolve” function in MATLAB spends 0.72 seconds to solve the HN model, and the maximal mismatches on both sides of (32) are limited within 10^{-10}. If an input check on the coefficient matrix (embedded in the “mldivide” function in MATLAB) is included to specify the most suitable solution algorithm, the computation time would come to 0.74 seconds. Overall, our improved formulation with the well-developed LU factorization method can effectively reduce the solution time and error.

Table II
COMPARISON OF THE COMPUTATION PERFORMANCES AMONG DIFFERENT SOLUTION METHODS IN CASE 2

Model formulation	Solution algorithm		Solution time (s)	Solution error
Basic	Decomposition-Iteration	Iterative	1.43	$\leq 10^{-5}$
Improved	Jacobi	Iterative	Unsolvable	
	Gauss-Seidel	Iterative	Unsolvable	
	Gauss Elimination	Non-iterative	Unsolvable	
	LU factorization (with partially pivoting)	Non-iterative	0.72	$\leq 10^{-10}$
	LU factorization (with partially pivoting and input check)	Non-iterative	0.74	$\leq 10^{-10}$

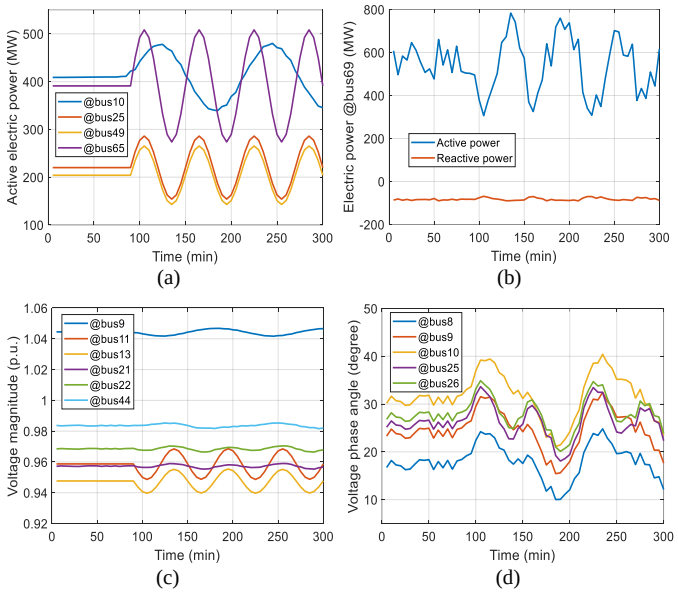

Figure 7. Energy flow results of PG: (a) Injected active power generations at cogeneration units (bus 10, 25, 49 and 65). (b) Power output variations of the slack bus (#69). (c) Voltage magnitude variation curves at some buses with more noticeable fluctuations. (d) Voltage phase angle variation curves at some buses with more noticeable fluctuations.

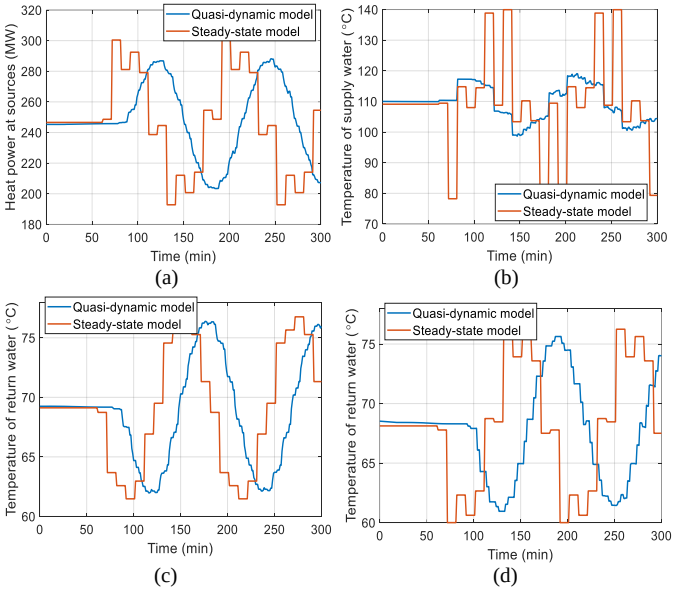

Figure 8. Comparison of energy flow results in HN1: (a) Heat power output of the slack node (#34). (b) Supply water temperature at Source 1 (node #1). (c) Return water temperature of the slack node (#34). (d) Return water temperature at node #59.

Some of the power flow results are displayed in Figure 7 to illustrate how the the states of HNs influence those of PG. The cogeneration units at bus 10, 25, 49 and 65 are all PV buses, with their generated active power given in Figure 7(a). The active power generations at bus 10 are determined by the heat power output of Source 2 in the first HN, with the heat-to-power ratio η^{bp} as 0.6. The power variations of the slack bus are shown in Figure 7(b), while the variations of voltage magnitudes and phase angles at some buses (with more noticeable fluctuations) are displayed in Figure 7(c) and (d). Basically, the active power fluctuations tend to have greater influence on the phase angles, while the reactive power fluctuations have more significant influence on the voltage magnitudes, so the fluctuations of phase angles are greater than those of voltage magnitudes. It should be noted that the reactive power consumptions at bus 11 and 15 are tenfold their actual values in order to illustrate the influence of reactive power injections on bus voltage magnitudes, as can be seen by the red and yellow curves in Figure 7(c).

C. Comparison between the steady-state and quasi-dynamic HN models

In Case 2, energy flow analysis of HN1 is carried out using both the steady-state and quasi-dynamic models. The results are comparatively displayed in Figure 8.

The heat power output at the slack node is shown in Figure 8(a), where the quasi-dynamic result witnesses a significant time delay compared with the steady-state one. Also, more detailed variations are captured with the quasi-dynamic model. Similar conclusions can be drawn from Figure 8(c) and (d), where the return water temperatures at the slack node and node #59 are respectively illustrated. As for the supply temperature of Source 1 shown in Figure 8(b), some outrageous points are observed where the steady-state result changes abruptly and differs from the quasi-dynamic one to an unacceptable extent — more than 20 °C.

In general, the difference between these two sets of energy flow results are quite significant, indicating a non-negligible level of error may be induced if using the steady-state model.

D. Tests on a larger real-life HN

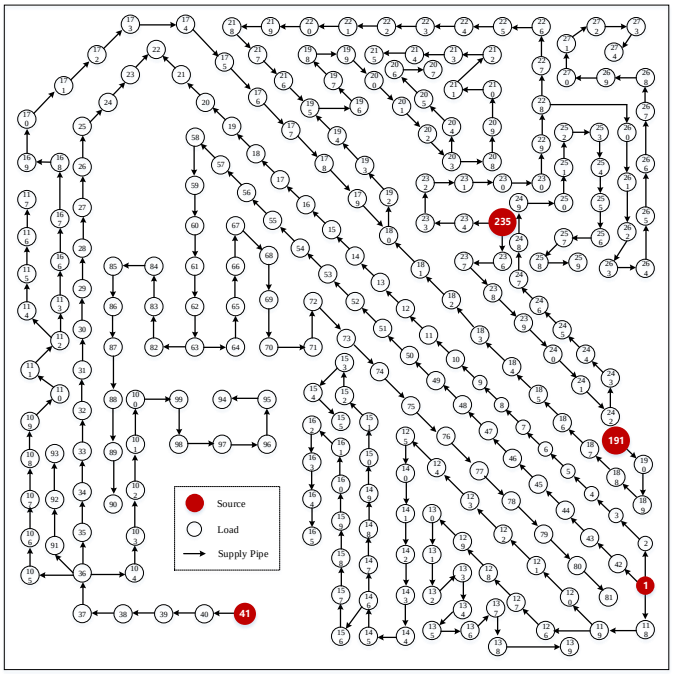

Figure 9. Diagram of the supply network in Case 3.

A more complex real-life HN located in Jiangsu, China is used here to further test the effectiveness and advantages of our improved model formulation and solution strategy. The supply network is sketched in Figure 9, where 4 sources co-deliver hot water to 270 loads. The supply and return networks contain 548 nodes and 820 pipes in total. Detailed parameters of this test case can be found in [37]. The overall simulation time is 24 hours and τ is 1 minute. Spatial difference step sizes h_i are set in the same way as in Case 2.

The computation performances among 6 different solution algorithms based on both the basic and improved model formulations are shown in Table III, where the LU factorization method only needs about 1/18 of the time consumed by the Decomposition-Iteration algorithm and maintains a lower level of error at the same time. From this case, we can see that our improved model formulation and solution strategy can improve the efficiency of energy flow calculation more significantly for long timescale simulation of large scale systems.

V. Conclusion

This paper develops a generic and efficient tool, MATHN, for quasi-dynamic energy flow calculation of an quality-regulated HN. After that, a generic solution framework that leverages MATPOWER and MATHN to realize decomposed energy flow analysis of PG and HN is further proposed.

The model reformulation work behind MATHN reduces the original loose form of the discretized HN model into a compact matrix equation, which slashes the problem scale by around 20 times and has better applicability. While the solution strategy behind it further converts the improved model formulation into a standard system of linear equations so that some existing well-recognized algorithms can be employed for fast and accurate solution. Case studies on 3 different scales of systems show that our work can substantially improve the generality, efficiency and accuracy of energy flow calculation.

However, at this stage the MATHN tool only applies to the quality-regulated HN. As one of our future focuses, we are trying to extend the function of MATHN to also being able to carry out quasi-dynamic energy flow calculation of the quantity-regulated HN.

VI. Further Discussion

There are a bunch of commercial tools for pipe flow simulation, including ANSYS, COMSOL, TRNSYS, etc. When it comes to calculating the energy flows of large-scale coupled energy networks, MATHN has the following two advantages.

Firstly, most of these commercial tools rely on a graphical interface to construct the investigated system — typically realized by dragging some library components onto a canvas, calibrating parameters, and further developing some connections among them. This is a user-friendly way of building small-scale system, but when the system contains hundreds of pipes and nodes, constructing such systems in commercial tools can be a time-consuming and challenging task. MATHN, on the other hand, is specifically designed to facilitate energy flow analysis of heating networks. It uses a formatted data file to collect the topology and parameters of the investigated networks, making it particularly suitable for analyzing large-scale networks. While we acknowledge that commercial tools may be able to accurately simulate single pipes or small-scale networks, MATHN's unique features allow for more convenient and efficient analysis of larger systems.

Secondly, many researchers and power engineers rely on the well-developed MATPOWER for power flow analysis of power grid. This means we will need to employ two separate tools to calculate the global energy flows of the coupled electric power and heating networks. Fortunately, MATHN is tailored to reduce the interaction burden with MATPOWER to a large extent. Because MATHN is based on MATLAB, the same development platform as MATPOWER, it is more easily integrated into existing workflows for researchers and engineers. With MATHN, users can conveniently calculate the energy flows of integrated electric power and heating networks, without the need for a complex execution code.

Acknowledgment

This work was supported by the National key Research and Development Program of China (2020YFE0200400) and the EPSRC through the project "Integrated heating and cooling networks with heat-sharing-enabled smart prosumers" (EP/T022795/1).

Last but not least, we would like to express our deep appreciation to Mr. Jonathan Marlow for his careful proof-reading and language polishing work, and to the China Scholarship Council, Dr. Tong Zhang, Mr. Suhan Zhang, and Mr. Ruizhi Yu for their generous help and professional support.

Table III
Comparison of the computation performances among different solution methods in Case 3

Model formulation	Solution algorithm		Solution time (s)	Solution error
Basic	Decomposition-Iteration	Iterative	1398.75	$\leq 10^{-5}$
Improved	Jacobi	Iterative	No solutions obtained	
	Gauss-Seidel	Iterative	Unsolvable	
	Gauss Elimination	Non-iterative	Unsolvable	
	LU factorization (with partially pivoting)	Non-iterative	74.60	$\leq 10^{-10}$
	LU factorization (with partially pivoting and input check)	Non-iterative	101.35	$\leq 10^{-10}$

REFERENCES

[1] J. Wu, J. Yan *et al.*, "Integrated energy systems," *Appl. Energy*, vol. 167, pp. 155–157, 2016.

[2] W. Gu, J. Wang *et al.*, "Optimal operation for integrated energy system considering thermal inertia of district heating network and buildings," *Appl. Energy*, vol. 199, pp. 234–246, 2017.

[3] C. Shao, Y. Ding *et al.*, "Modeling and integration of flexible demand in heat and electricity integrated energy system," *IEEE Trans. Sustain. Energy*, vol. 9, no. 1, pp. 361–370, 2018.

[4] Z. Pan, J. Wu *et al.*, "Quasi-dynamic interactions and security control of integrated electricity and heating systems in normal operations," *CSEE J. Power Energy Syst.*, vol. 5, no. 1, pp. 120–129, 2019.

[5] L. Wang, J. Zheng *et al.*, "Multi-time scale dynamic analysis of integrated energy systems: An individual-based model," *Appl. Energy*, vol. 237, pp. 848–861, 2019.

[6] X. Qin, H. Sun *et al.*, "A generalized quasi-dynamic model for electric-heat coupling integrated energy system with distributed energy resources," *Appl. Energy*, vol. 251, p. 113270, 2019.

[7] J. Yang, N. Zhang *et al.*, "On an equivalent representation of the dynamics in district heating networks for combined electricity-heat operation," *IEEE Trans. Power Syst.*, vol. 35, no. 1, pp. 560–570, 2020.

[8] S. Yao, W. Gu *et al.*, "Dynamic energy flow analysis of the heat-electricity integrated energy systems with a novel decomposition-iteration algorithm," *Appl. Energy*, vol. 322, p. 119492, 2022.

[9] I. B. Hassine and U. Eicker, "Simulation and optimization of the district heating network in scharnhauser park," in *Proceedings of the 2nd Polygeneration Conference*, Tarragona, 2011, pp. 1–18.

[10] X. Liu, J. Wu *et al.*, "Combined analysis of electricity and heat networks," *Applied Energy*, vol. 162, pp. 1238 – 1250, 2016.

[11] P. He, G. Sun, H. Wu *et al.*, *Heating engineering*. China Architecture Press, 2009.

[12] K. Li, Hang Hou *et al.*, "Probabilistic energy flow calculation for regional integrated energy system considering cross-system failures," *Appl. Energy*, vol. 308, p. 118326, 2022.

[13] Q. Hu, Y. Liang *et al.*, "Topological partition based multi-energy flow calculation method for complex integrated energy systems," *Energy*, vol. 244, no. 123152, 2022.

[14] H. R. Massrur, T. Niknam *et al.*, "Investigation of carrier demand response uncertainty on energy flow of renewable-based integrated electricity-gas-heat systems," *IEEE Trans. Ind. Informat.*, vol. 14, no. 11, pp. 5133–5142, 2018.

[15] ——, "Fast decomposed energy flow in large-scale integrated electricity-gas-heat energy systems," *IEEE Trans. Sustain. Energy*, vol. 9, no. 4, pp. 1565–1577, 2018.

[16] D. Chen, X. Hu *et al.*, "Nodal-pressure-based heating flow model for analyzing heating networks in integrated energy systems," *Energy Conv. Manag.*, vol. 206, 2020.

[17] S. Zhang, W. Gu *et al.*, "Partitional decoupling method for fast calculation of energy flow in a large-scale heat and electricity integrated energy system," *IEEE Trans. Sustain. Energy*, vol. 12, no. 1, pp. 501–513, 2021.

[18] A. Benonysson, "Dynamic modeling and operational optimization of district heating system," Ph.D. dissertation, Tech. Uni. Denmark, Lyngby, 1991.

[19] Z. Li, W. Wu *et al.*, "Combined heat and power dispatch considering pipeline energy storage of district heating network," *IEEE Trans. Sustain. Energy*, vol. 7, no. 1, pp. 12–22, 2016.

[20] S. Lu, W. Gu *et al.*, "Thermal inertial aggregation model for integrated energy systems," *IEEE Trans. Power Syst.*, vol. 35, no. 3, pp. 2374–2387, 2020.

[21] V. D. Stevanovic, B. Zivkovic *et al.*, "Prediction of thermal transients in district heating systems," *Energy Conv. Manag.*, vol. 50, no. 9, pp. 2167–2173, 2009.

[22] B. Chen, H. Sun *et al.*, "Energy circuit theory of integrated energy system analysis (iii): steady and dynamic energy flow calculation," *CSEE J. Power Energy Syst.*, vol. 40, no. 15, pp. 4820–4831, 2020.

[23] J. Li, Y. Huang *et al.*, "Gradient descent iterative method for energy flow of integrated energy system considering multiple modes of compressors," *Energy Conv. Manag.*, vol. 207, no. 100, p. 112534, 2020.

[24] D. Chen, X. Hu *et al.*, "Nodal-pressure-based heating flow model for analyzing heating networks in integrated energy systems," *Energy Conv. Manag.*, vol. 206, p. 112491, 2020.

[25] A. S. Haghighi and A. R. Seifi, "An integrated steady-state operation assessment of electrical, natural gas, and district heating networks," *IEEE Trans. Power Syst.*, vol. 31, no. 5, pp. 3636–3647, 2016.

[26] G. T. Ayele, P. Haurant *et al.*, "An extended energy hub approach for load flow analysis of highly coupled district energy networks: Illustration with electricity and heating," *Appl. Energy*, vol. 212, pp. 850–867, 2018.

[27] Q. Sun, Q. Dong *et al.*, "A unified energy flow analysis considering initial guesses in complex multi-energy carrier systems," *Energy*, vol. 213, p. 118812, 2020.

[28] H. Tian, H. Zhao *et al.*, "A dual-driven linear modeling approach for multiple energy flow calculation in electricity-heat system," *Appl. Energy*, vol. 314, 2022.

[29] Z. Pan, Q. Guo *et al.*, "Interactions of district electricity and heating systems considering time-scale characteristics based on quasi-steady multi-energy flow," *Appl. Energy*, vol. 167, pp. 230–243, 2016.

[30] G. Zhang, F. Zhang *et al.*, "A fixed-point based distributed method for energy flow calculation in multi-energy systems," *IEEE Trans. Sustain. Energy*, vol. 11, no. 4, pp. 2567–2580, 2020.

[31] H. R. Massrur, T. Niknam *et al.*, "Fast decomposed energy flow in large-scale integrated electricity-gas-heat energy systems," *IEEE Trans. Sustain. Energy*, vol. 9, no. 4, pp. 1565–1577, 2018.

[32] G. Sun, W. Wang *et al.*, "Rapid energy flow calculation method for integrated electrical and thermal systems," *Int. J. Electr. Power Energy Syst.*, vol. 123, p. 106317, 2020.

[33] P. Gao, X. Zhou *et al.*, "Sequence iterative method-based steady-state analysis of integrated electricity, gas and heating networks," *Int. J. Electr. Power Energy Syst.*, vol. 124, p. 106359, 2021.

[34] R. D. Zimmerman, C. E. Murillo-Sánchez *et al.*, "Matpower: Steady-state operations, planning, and analysis tools for power systems research and education," *IEEE Trans. Power Syst.*, vol. 26, no. 1, pp. 12–19, 2011.

[35] S. Yao, W. Gu *et al.*, "Dynamic optimal energy flow in the heat and electricity integrated energy system," *IEEE Trans. Sustain. Energy*, vol. 12, no. 1, pp. 179–190, 2021.

[36] CHPQA, "GUIDANCE NOTE 28: the determination of Z ratio." [Online]. Available: https://www.chpqa.com/guidance_notes/GUIDANCE_NOTE_28.pdf

[37] S. Yao. (2022) Mathn: shared codes and data. [Online]. Available: https://doi.org/10.24433/CO.7016208.v1

[38] ——. (2022) Case1: an illustrative case. [Online]. Available: https://www.jianguoyun.com/p/DQ9hSgcQ8su3BxiqitIEIAA